Journal of
Applied Crystallography
ISSN 0021-8898

Received 16 August 2006
Accepted 22 December 2006

Grazing-incidence small-angle X-ray scattering studies on templating nanopores in networked polymer thin films with a multi-armed porogen

Kyeong Sik Jin,‡ Kyuyoung Heo,‡ Weontae Oh, Jinhwan Yoon, Byeongdu Lee, Yongtaek Hwang, Jong-Seong Kim, Young-Hee Park, Kwang-Woo Kim, Jehan Kim, Taihyun Chang and Moonhor Ree*

Department of Chemistry, Pohang Accelerator Laboratory, National Research Laboratory for Polymer Synthesis and Physics, Center for Integrated Molecular System, and BK School of Molecular Science, Pohang University of Science and Technology, Pohang 790-784, Republic of Korea. Correspondence e-mail: ree@postech.edu

The mechanism of thermal pore generation in organosilicate thin films loaded with a six-armed star-shaped poly(ϵ-caprolactone) porogen was quantitatively investigated by using *in-situ* grazing-incidence small-angle X-ray scattering and thermogravimetry. These analyses found that the blend components have a limited miscibility that depends on the composition; for porogen loadings up to only 20 wt%, molecularly miscible blend films were obtained. Even for the miscible blend films, heating the films produced a curing reaction of the precursor matrix component, leading to the phase separation of the porogen component. This phase separation was found to begin at 393 K for 10 wt% porogen loaded films and at 373 K for 20 wt% porogen loaded films, and to continue for temperatures up to 423 K. The porogen aggregates remained and were confined within the matrix film without any further growth or movement until complete thermal decomposition above 564 K.

1. Introduction

In order to scale down the feature size of integrated circuits (ICs), significant reductions in the dielectric constants of the interdielectric layers in these devices are required. Reducing the cross-sectional areas of interconnects increases the resistance of the metal conductor wiring and narrowing the spacing between interconnects also increases the capacitance, which result in severe device performance limitations. Thus the microelectronics industry requires low dielectric constant (low-k) materials because such dielectrics can not only lower line-to-line noise in interconnect conductors but can also minimize power dissipation issues by reducing the capacitance between the interconnects (Czornyj *et al.*, 1992; Maex *et al.*, 2003; Maier, 2001; Morgen *et al.*, 2000; Ree *et al.*, 1995, 2006).

Since the dielectric constant of air is k = 1.01, which is the lowest value attainable, there is significant interest in incorporating air into dielectric materials in order to reduce their dielectric constants, *i.e.*, in producing low-k porous interdielectric materials (Maex *et al.*, 2003; Morgen *et al.*, 2000; Ree *et al.*, 1995, 2006). One major approach to the development of low-k porous dielectric materials is the templated polycondensation of soluble organosilicate precursors in the presence of a thermally labile, organic polymeric porogen, with the subsequent formation of pores in the resulting dielectrics through the sacrificial thermal decomposition of the porogen (Bolze *et al.*, 2001; Maex *et al.*, 2003; Magbitang *et al.*, 2005; Morgen *et al.*, 2000; Lee, Park, Hwang *et al.*, 2005; Lee, Yoon *et al.*, 2005; Oh *et al.*, 2003; Lee, Oh *et al.*, 2005; Nguyen *et al.*, 1999; Ree *et al.*, 2006). However, the tendency of porogens to aggregate in organosilicates increases the pore size and porosity of the resulting dielectrics (Bolze *et al.*, 2001; Magbitang *et al.*, 2005; Lee, Park, Hwang *et al.*, 2005; Lee, Yoon *et al.*, 2005; Oh *et al.*, 2003; Lee, Oh *et al.*, 2005; Nguyen *et al.*, 1999; Ree *et al.*, 2006); when the size of porogen aggregates approaches the critical feature size, the resulting porous dielectrics become unsuitable for use in the production of ICs. A large number of arms of star-shaped porogens has been found to result in severe aggregation even with a 10 wt% porogen loading, generating large, interconnected pores in dielectric thin films (Bolze *et al.*, 2001; Magbitang *et al.*, 2005; Lee, Yoon *et al.*, 2005; Oh *et al.*, 2003; Lee, Oh *et al.*, 2005; Nguyen *et al.*, 1999). Thus, the development of advanced ICs requires a method for generating a uniform distribution of closed pores with dimensions significantly smaller than the feature size of dielectric materials. Moreover, the ability to characterize the pore structure of porous dielectric thin films is as important as developing the dielectrics and porogens themselves. It is also necessary to understand the mechanism of pore generation in such dielectric materials. Recently the pore generation in organosilicate dielectric films with a thermally labile four-armed poly(ϵ-caprolactone) porogen was first investigated by *in-situ* grazing-incidence small-angle X-ray scattering (GISAXS) analysis using synchrotron radiation sources (Lee, Yoon *et al.*, 2005).

In the present study, we extended *in-situ* GISAXS analysis to blend films of a six-armed star-shaped poly(ϵ-caprolactone) (PCL6) porogen and a polymethylsilsesquioxane (PMSSQ) dielectric precursor. In addition to the *in-situ* GISAXS analysis, the thermal properties of the PCL6 porogen, the PMSSQ dielectric precursor and their blends were investigated with thermogravimetric analysis (TGA). The obtained porous thin films were examined by transmission electron microscopy (TEM). These studies provided new insights into the miscibility of, and phase separation in, the blends of the

‡ K. S. Jin and K. Heo contributed equally to this work.

PMSSQ dielectric precursor and PCL6 porogen, and further into the mechanism of this method of pore templating. Further, these studies provided information on the effect of the arm number of the porogen in the pore generation mechanism.

2. Experimental

A soluble PMSSQ precursor [10 000 $\overline{M}_w$ (weight-average molecular weight), GR650F] was supplied by Techneglass (Perrysburg, OH, USA). A PCL6 porogen of 8 100 $\overline{M}_w$ with a polydispersity index (PDI) of 1.11 and an average degree of polymerization per arm ($\overline{DP}$/arm) of 7.9 was synthesized according to a procedure described elsewhere (Bolze *et al.*, 2001; Lee, Yoon *et al.*, 2005; Nguyen *et al.*, 1999; Shin *et al.*, 2001). A series of homogeneous solutions of PCL6 porogen and PMSSQ precursor were prepared in methyl isobutyl ketone (MIBK) (5 wt% solid content) using porogen compositions in the range 0–40 wt%. Each solution was filtered using a polytetrafluoroethylene (PTFE) membrane filter of pore size 0.2 µm, and spin-coated onto precleaned silicon [Si(100)] substrates at 3000 r.p.m. for 30 s, which were then dried at 323 K for 1 h under a nitrogen atmosphere and in vacuum at room temperature for 1 day. The dried films were found to have thicknesses in the range 100–150 nm by using a spectroscopic ellipsometer (Model VASE, Woollam, Lincoln, NE).

In-situ GISAXS measurements were carried out at the 4C1 and 4C2 beamlines of the Pohang Accelerator Laboratory (PAL) (Bolze *et al.*, 2002; Lee *et al.*, 2004; Ree & Ko, 2005; Yu *et al.*, 2005). A monochromated X-ray radiation source with wavelength λ = 0.171 nm and a two-dimensional (2D) charge-coupled device (CCD) detector (Roper Scientific, Trenton, NJ) were used. The sample-to-detector distance was 2500 mm. Aluminium foil strips were employed as semi-transparent beam stops because the intensity of specular reflection from the substrate is much stronger than the intensity of GISAXS near the critical angle. Each film sample was mounted on a home-made z-axis goniometer equipped with a vacuum chamber. The incidence angle α_i of each X-ray beam was set in the range 0.20–0.22°, which is between the critical angles of the films and the Si substrate ($\alpha_{c,f}$ and $\alpha_{c,s}$). The film samples were heated to 673 K at a rate of 2.0 K min^{-1}, and subsequently kept at that temperature for 30 min under vacuum. Thereafter, the films were cooled to room temperature at a rate of 2.0 K min^{-1} under vacuum. Each measurement was collected for 145 s. Data correction was carried out with respect to the background scattering and the intensity decay of incident primary X-rays during measurements. Scattering angles were corrected by the positions of X-ray beams reflected from the silicon substrate interface with changing incidence angle α_i and from a precalibrated polystyrene-b-polyethylene-b-polybutadiene-b-polystyrene copolymer. TGA was conducted with a heating rate of 2.0 K min^{-1} under a nitrogen atmosphere for the dried films as well as for the PMSSQ precursor and PCL6 porogen by using a Seiko TG/DT analyzer (Model EXSTAR 6000 TG/DT, Tokyo, Japan) over the range 303–1073 K; this heating rate was the same as that chosen for the *in-situ* GISAXS measurements. In addition, TEM measurements were carried out using a JEM microscope (model 4000Fx) on samples prepared on carbon grids of 400 mesh by dip-coating in dilute solutions (1.0 wt% solid content).

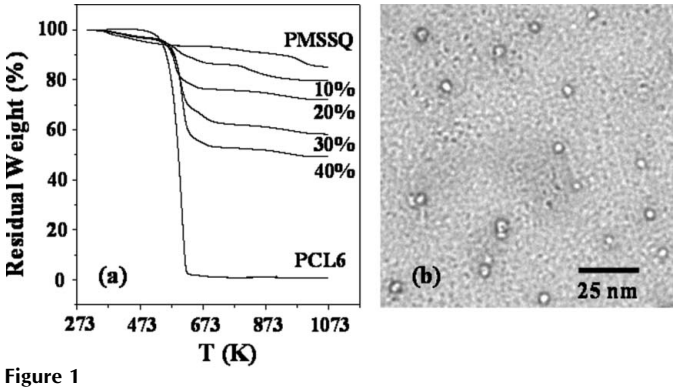

Figure 1
(*a*) TGA thermograms of the PMSSQ precursor, PCL6 porogen, and blend samples. The measurements were carried out at a heating rate of 2.0 K min^{-1} under a nitrogen atmosphere. (*b*) TEM image of a nanoporous PMSSQ dielectric prepared from a PMSSQ precursor sample loaded with 10.0 wt% PCL6 porogen.

3. Results and discussion

The TGA results are shown in Fig. 1(*a*). As can be seen in the figure, on heating at 2.0 K min^{-1} in nitrogen ambient the PMSSQ precursor undergoes weight losses between 348 and 613 K, which are due to the loss of the water and ethanol byproducts of its thermal curing reaction. The cured PMSSQ product finally undergoes thermal decomposition above 773 K. In contrast, the PCL6 porogen decomposes above 519 K, with complete decomposition above 629 K leaving no residue (Fig. 1a). However, when the PCL6 porogen is embedded within the PMSSQ precursor matrix, the porogen's thermal decomposition commences around 564 K, *i.e.* this is the onset temperature of thermal degradation ($T_{d,p}$) of the PCL6 porogen in the PMSSQ precursor matrix, and this does not vary for porogen loadings in the range 10–40 wt%. This increase in the decomposition temperature is thought to be due to the covalent reaction of the porogen hydroxyl end groups with the ethoxy and hydroxyl groups of the PMSSQ precursor prior to porogen decomposition.

Fig. 1(*b*) shows a representative TEM image of a porous PMSSQ film. The TEM image clearly shows that the nanopores generated in the dielectric film by the sacrificial thermal degradation of the star-shaped PCL6 porogen are spherical in shape and that their sizes are around 6 nm.

Taking these TGA and TEM results into account, *in-situ* 2D GISAXS measurements were carried out on thin films of the PMSSQ precursor loaded with various amounts of the PCL6 porogen, which were heated up to 673 K at a rate of 2.0 K min^{-1}, kept at that temperature for 30 min, and then cooled to room temperature; the thermal processes were conducted in vacuum.

Fig. 2 shows a typical 2D GISAXS pattern, which was measured *in-situ* during the heat treatment of a PMSSQ precursor film loaded with 10 wt% PCL6 porogen. As shown in the figure, the in-plane and out-of-plane GISAXS profiles were extracted at $\alpha_f = 0.17°$ and $2\theta_f = 0.25°$

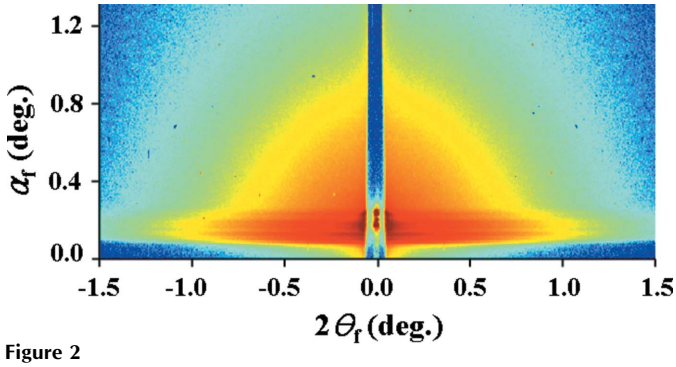

Figure 2
2D GISAXS pattern measured at $\alpha_i = 0.20°$ for a 100 nm thick porous PMSSQ film prepared with a PCL6 loading of 10 wt%.

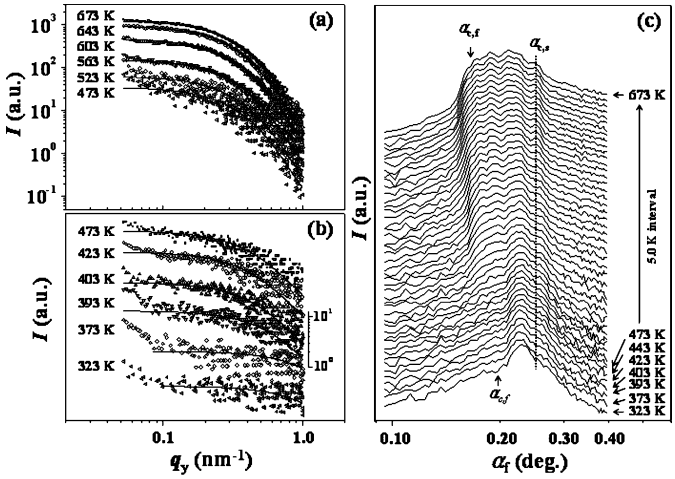

Figure 3
(*a*), (*b*) In-plane scattering profiles at $\alpha_f = 0.17^\circ$ and (*c*) out-of-plane scattering profiles at $2\theta_f = 0.25^\circ$ of 2D GISAXS patterns obtained during heating (2.0 K min^{-1}) of a PMSSQ precursor film loaded with 10 wt% PCL6 porogen under vacuum: the symbols represent the measured data, and the solid lines were obtained by fitting the data with the GISAXS formula. $\alpha_{c,f}$ and $\alpha_{c,s}$ indicate the critical angles of the dielectric film and Si substrate respectively.

respectively, where α_f is the angle between the scattered beam and the film surface (*i.e.*, the out-of-plane exit angle) and $2\theta_f$ is the angle between the scattered beam and the plane of incidence (*i.e.*, the in-plane exit angle). These one-dimensional scattering profile extractions were carried out for all the *in-situ* measured 2D GISAXS patterns. Representative sets of the in-plane and out-of-plane GISAXS profiles extracted from the 2D GISAXS patterns obtained *in-situ* for a PMSSQ precursor film loaded with 10 wt% PCL6 are displayed in Figs. 3(*a*) and 3(*b*). Similar sets of in-plane and out-of-plane GISAXS profiles were obtained for the PMSSQ precursor films loaded with >10 wt% PCL6 (data not shown).

We attempted to quantitatively analyze the extracted in-plane GISAXS (I_{GISAXS}) profiles by using the following recently derived GISAXS formula (Lee, Yoon *et al.*, 2005; Lee, Park, Yoon *et al.*, 2005):

$$\begin{aligned} I_{GISAXS}(\alpha_f, 2\theta_f) \simeq \frac{1}{16\pi^2}\frac{1-\exp[-2\mathrm{Im}(q_z)d]}{2\mathrm{Im}(q_z)} \\ \times \Big\{ \left|T_i T_f\right|^2 I_1[q_{||}, \mathrm{Re}(q_{1,z})] \\ + \left|T_i R_f\right|^2 I_1[q_{||}, \mathrm{Re}(q_{2,z})] \\ + \left|T_f R_i\right|^2 I_1[q_{||}, \mathrm{Re}(q_{3,z})] \\ + \left|R_i R_f\right|^2 I_1[q_{||}, \mathrm{Re}(q_{4,z})] \Big\}, \end{aligned} \quad (1)$$

where $\mathrm{Im}(q_z) = |\mathrm{Im}(k_{z,f})| + |\mathrm{Im}(k_{z,i})|$, $\mathrm{Re}(x)$ is the real part of x, d is the film thickness, R_i and T_i are the reflected and transmitted amplitudes of the incoming X-ray beam, respectively, and R_f and T_f are the reflected and transmitted amplitudes of the outgoing X-ray beam, respectively. In addition, $q_{||} = (q_x^2 + q_y^2)^{1/2}$, $q_{1,z} = k_{z,f} - k_{z,i}$, $q_{2,z} = -k_{z,f} - k_{z,i}$, $q_{3,z} = k_{z,f} + k_{z,i}$ and $q_{4,z} = -k_{z,f} + k_{z,i}$; here, $k_{z,i}$ is the z component of the wave vector of the incoming X-ray beam, which is given by $k_{z,i} = k_o(n_R^2 - \cos^2\alpha_i)^{1/2}$, and $k_{z,f}$ is the z component of the wave vector of the outgoing X-ray beam, which is given by $k_{z,f} = k_o(n_R^2 - \cos^2\alpha_f)^{1/2}$, where $k_o = 2\pi/\lambda$, λ is the wavelength of the X-ray beam, n_R is the refractive index of the film given by $n_R = 1 - \delta + i\xi$ with dispersion δ and absorption ξ, α_i is the out-of-plane grazing incident angle of the incoming X-ray beam, and α_f is the out-of-plane exit angle of the outgoing X-ray beam. q_x, q_y and q_z are the components of the scattering vector $\mathbf{q}$. I_1 is the scattering intensity of the porogens or pores in the film.

In our analysis of the GISAXS data with this formula, we examined all possible scattering models (sphere, cylinder, disc *etc.*) for the scattering intensity [*i.e.*, the I_1 term in equation (1)] from the porogens or pores in the films. We found that the following equation for I_1 derived under kinematic theory is the most suitable for analyzing the scattering data with the GISAXS formula:

$$I_1 = c\int_0^\infty n(r)v(r)^2|F(qr)|^2 S(qr)\,\mathrm{d}r, \quad (2)$$

where c is a constant, q is the magnitude of the scattering vector $\mathbf{q}$, $v(r)$ is the volume of each pore, $F(qr)$ is the spherical form factor, and $S(qr)$ is the structure factor for the hard-sphere model (Kinning & Thomas, 1984; Pedersen, 1994). $n(r)$ is the lognormal size distribution function of the porogens or pores:

$$n(r) = \frac{1}{(2\pi)^{1/2} r_o \sigma \exp(\sigma^2/2)} \exp[-\ln(r/r_o)^2/2\sigma^2], \quad (3)$$

where r is the pore radius, and r_o and σ are the pore radius corresponding to the peak maximum and the width of the pore radius distribution, respectively.

As can be seen in Figs. 3(*a*) and 3(*b*), the in-plane GISAXS scattering profiles can be satisfactorily fitted with the GISAXS formula combined with equations (2) and (3), indicating that the porogens and their template pores in the dielectric films have a spherical shape. In these fittings we in fact considered all possible packing structures for the structure factor $S(qr)$, and then found that only a randomly packed structure of spheres fits the scattering data well, showing that the porogen molecules (or porogen aggregates) as well as their imprinted pores are randomly dispersed in the film. The results of the analyses of these scattering profiles are summarized in Fig. 4.

As can be seen in Fig. 3(*b*), during the heating run the PMSSQ film loaded with 10 wt% PCL6 porogen produces a very weak scattering profile at 323 K, and exhibits similar scattering profiles up to near 393 K. Consider a single molecule of PCL6 porogen under theta conditions. The average radius of gyration ($\overline{R}_g$) of the PCL6 porogen can be calculated from its molecular weight by using $\overline{DP}$/arm = 7.9. We estimate that $\overline{R}_g$ of the single porogen molecule is 2.25 nm from the molecular weight; from this $\overline{R}_g$ value, we can further estimate the radius (r_o) of the single porogen molecule corresponding to the peak maximum in the radius distribution, the width of the radius distribution (σ) and the average radius ($\bar{r}$): $r_o = 1.41$ nm, $\sigma = 0.30$ and $\bar{r} = 1.61$ nm. With these molecular size parameters we attempted to fit the scattering profiles obtained below 393 K by using the GISAXS formula. As shown in Fig. 3(*b*), the scattering profiles measured at

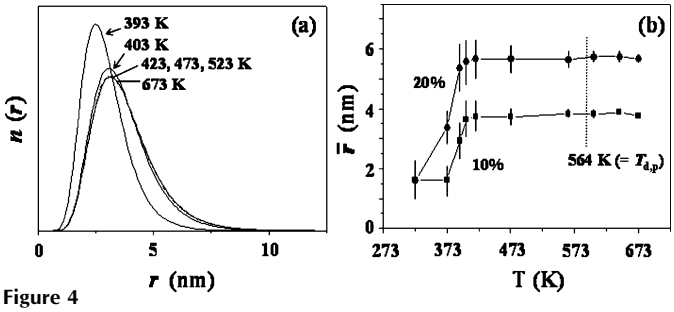

Figure 4
(*a*) Porogen and pore radii and their radius distributions determined from the GISAXS analysis of the in-plane scattering profile data in Figs. 3(*a*) and 3(*b*). (*b*) Average radii of porogens and pores in the PMSSQ films determined from the GISAXS analysis of the in-plane scattering profile data obtained for the films loaded with 10 and 20 wt% PCL6 porogen.

323 and 373 K, as the representative examples of the scattering profiles measured below 393 K, are satisfactorily fitted with the GISAXS formula, particularly in the q range 0.1–1.0 nm^{-1}. These results suggest that the PCL6 molecules are molecularly dispersed in the PMSSQ precursor film loaded with 10 wt% porogen, which was prepared by spin coating the homogeneous solution in MIBK and subsequent drying at 323 K, and such molecular dispersion of the porogen is retained up to near 393 K. Indeed, the observed weak scattering profiles are attributed to the thorough dispersion of single porogen molecules within the PMSSQ precursor film. Such weak scattering profiles are also attributed to a relatively low contrast in the electron densities of the PMSSQ precursor and porogen.

However, the analysis of the scattering profile measured at 393 K, which is still weak in intensity but does have a different shape from those measured below 393 K, indicates that the PCL6 porogen in the film has $\bar{r}$ = 2.93 nm with σ = 0.33. These $\bar{r}$ and σ values are greater than those ($\bar{r}$ = 1.61 nm and σ = 0.30) of a single porogen molecule, indicating that during the heating run the porogen component of the PMSSQ film loaded with 10 wt% PCL6 porogen starts to undergo phase separation around 393 K and then forms aggregates with $\bar{r}$ = 1.61 nm and σ = 0.33. Such porogen phase separation continues up to 423 K, forming larger porogen aggregates ($\bar{r}$ = 3.73 nm and σ = 0.35) (Fig. 4). With further increases in the temperature, however, the porogen aggregates approximately maintain their size and size distribution until they undergo thermal degradation (Fig. 4).

These phase separations of the porogen component can be understood by considering the thermal characteristics of the PMSSQ precursor and porogen components. PMSSQ precursors were recently reported to have glass transition temperatures T_g in the range 361–384 K, depending on the ratio of hydroxyl and ethoxy groups within the precursors (Oh, 2003); a similar T_g is expected for the PMSSQ precursor used in our study. As determined from the TGA results discussed above, during the heating run the PMSSQ precursor matrix undergoes a slow curing reaction over the temperature range 348–613 K, forming crosslinks. This curing reaction of the PMSSQ precursor component is enhanced by the increase in molecular mobility that occurs due to thermal heating during the heating run. As the curing reaction proceeds, the degree of crosslinking of the PMSSQ precursor increases, which produces increases in its glass transition temperature T_g and in the restriction of molecular mobility. In contrast, the PCL6 porogen component (which has a melting point T_m of 300 K and a T_g of 203 K) (Oh, 2003) appears highly mobilized during the heating run. The observed phase separation of the porogen component is thus first induced by segregation of the PMSSQ precursor component due to its curing reaction, which results from the heating. These induced phase separations of both components continue with increases in the temperature. In particular, the phase separation of the PCL6 porogen component occurs readily up to 423 K, but becomes restricted immediately above this temperature, due to the immobilization of the PMSSQ precursor matrix caused by the formation of crosslinks and by its resulting high T_g.

Above 564 K, the intensity of the scattering profile was found to increase with increasing temperature (up to 673 K) while retaining its shape (Fig. 3a). These increases in intensity with temperature are attributed to pores created in the film by the thermal degradation of the porogen aggregates above 564 K. From an analysis of the scattering profiles, the size and size distribution of pores generated in the film were found to be almost identical to those of the porogen aggregates developed up to around 423 K (Fig. 4). These results indicate that above 564 K the porogen aggregates confined within the immobilized PMSSQ precursor matrix undergo sacrificial thermal firing without further aggregation. This ultimately results in the template of pores within the cured matrix film, with sizes equivalent to those of the porogen aggregates.

The quantitative analysis of the scattering data with the GISAXS formula was extended to the in-plane GISAXS profiles obtained during heat treatment of the PMSSQ precursor films loaded with 20 wt% PCL6 porogen. The results of the analysis of the experimental scattering profiles are summarized in Fig. 4. Only two differences were observed between the results for this film composition and those obtained for the film loaded with 10 wt% porogen. First, the phase separation of the porogen resulting from curing of the PMSSQ precursor matrix was found to commence at 373 K, which is lower than that (393 K) of the 10 wt% porogen loaded composite film. Second, the porogen aggregates developed in the film were found to have larger sizes and broader size distributions than those of the 10 wt% porogen loaded film.

In contrast to the results for the films presented above, the scattering profiles of the films prepared with higher porogen loadings (30–40 wt%) could not be fitted with the GISAXS formula; the porogen aggregates in these films are too large and are thus outside the detection limits of the GISAXS setup used in our study. These results indicate that at higher porogen loadings, the porogen molecules in the PMSSQ precursor film undergo significant phase separation during the film formation process, in particular during the spin-coating and subsequent drying steps, *i.e.*, even before the heating run, resulting in the formation of large porogen aggregates with broad size distributions.

The above results collectively indicate that the PCL6 porogen molecules have a tendency to aggregate in the PMSSQ precursor matrix, a tendency that is enhanced as the porogen loading is increased and also as the degree of crosslinking in the PMSSQ precursor component increases with temperature on heating. A similar porogen aggregation tendency was previously observed for the four-armed poly(ϵ-caprolactone) (PCL4) porogen loaded in PMSSQ dielectric films (Lee, Yoon *et al.*, 2005), which has an average arm length ($\overline{DP}$/arm = 8.9) very close to that ($\overline{DP}$/arm = 7.9) of the PCL6 porogen. Moreover, surprisingly, it was found that the nanopores templated in the PMSSQ dielectric films with the PCL6 porogen have a similar size and size distribution as observed in the nanopores created in the dielectric films by the equivalent amount of the PCL4 porogen.

However, the onset aggregation temperature in the 10 wt% PCL6 loaded film of the present study is 30 K lower than that (423 K) observed in the PMSSQ dielectric film loaded with the equivalent amount of the PCL4 porogen ($\overline{DP}$/arm = 8.9) (Lee, Yoon *et al.*, 2005). Furthermore, for the 20 wt% porogen loaded films, the onset aggregation temperature of the PCL6 porogen is 35 K lower than that (408 K) of the PCL4 porogen (Lee, Yoon *et al.*, 2005). These results collectively show that in the PMSSQ films loaded with star-shaped PCL porogens, aggregations of the porogen component induced by the thermal curing reaction of the PMSSQ precursor component during the thermal process are influenced by the arm number of the porogen. Such porogen aggregation tends to start at a lower temperature as the arm number of the porogen increases and as the loading amount of the porogen increases.

From the experimental in-plane GISAXS profiles we also attempted to determine the invariant Q, which is the integrated area of a scattering profile with respect to the measured q range; here, Q is proportional to the product of the volume fractions of the PMSSQ and porogen components and the difference between the squared electron densities of the two components of the film. The resulting invariant Q values are plotted in Fig. 5. As can be seen in the figure, Q

is small at room temperature, and is independent of the porogen loading as well as of the degree of porogen aggregation in the PMSSQ precursor films, which is principally due to the relatively low contrast between the electron densities of the porogen and PMSSQ precursor components. However, Q increases very slowly with increases in temperature during the heating run. Q increases rapidly around 564 K (= $T_{d,p}$), and continues to rise up to 673 K. These results provide important information about films in which the porogen undergoes sacrificial thermal degradation, generating pores, and the PMSSQ precursor undergoes curing. These results are in good agreement with the TGA results described above. Almost the same $T_{d,p}$ value (563 K) was observed for the PCL4 porogen loaded in the PMSSQ film (Lee, Yoon *et al.*, 2005). These results indicate that there is apparently no effect of arm number on the thermal degradation of star-shaped poly(ϵ-caprolactone) porogens with similar length of arms in PMSSQ films.

In addition to the in-plane scattering data analysis, the extracted out-of-plane GISAXS profiles were analyzed. As can be seen in Fig. 3(*c*), the scattering profile obtained at 323 K appears very weak, which is attributed to the lack of electron density contrast between the porogen and PMSSQ precursor components. From this scattering profile, the critical angle of the film $\alpha_{c,f}$ was estimated to be 0.194°; the critical angle of the silicon substrate $\alpha_{c,s}$ is 0.245°. With increasing temperature, a variation of $\alpha_{c,f}$ is clearly evident, but $\alpha_{c,s}$ does not appear to vary (Fig. 3*c*). $\alpha_{c,f}$ decreases slowly as the temperature draws closer to 564 K. This is due to the removal of water and ethyl alcohol, which are formed in the film as byproducts of the curing of the PMSSQ precursor component. Above 564 K, $\alpha_{c,f}$ decreases significantly as the temperature is increased, achieving a final value of 0.171° at 673 K. This drastic shift in $\alpha_{c,f}$ is attributed primarily to the reduction in the electron density of the film that occurs when pores are generated in the film as a result of the thermal degradation of the porogen aggregates, but also to the removal of the water and ethyl alcohol byproducts from the film. Similar trends in $\alpha_{c,f}$ with temperature were observed for the out-of-plane GISAXS profiles of the films with different compositions (data not shown). The porosities of the obtained porous films were found to be in the range 14.4–42.7%, depending on the initial porogen loadings; higher initial porogen loadings of the PMSSQ precursor film resulted in porous dielectric films with higher porosities.

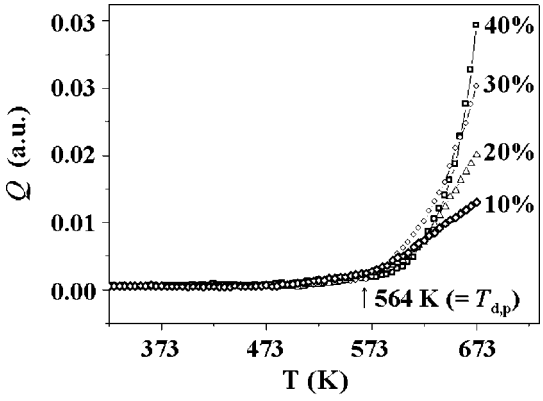

Figure 5
Temperature dependence of the invariant Q values obtained from in-plane GISAXS (which was extracted at α_f = 0.17°) of 2D GISAXS patterns obtained during heating at 2.0 K min^{-1} of blend films of PMSSQ precursor and PCL6 porogen in various compositions under vacuum. The notation used indicates the initial porogen loading in wt%.

4. Conclusions

The *in-situ* GISAXS data analysis of the present study established a mechanism for the formation of pores within the PMSSQ films containing the PCL6 porogen.

The porogen was found to be miscible with the PMSSQ precursor film for loadings up to 20 wt%. Thermal processing of the miscible blends caused a curing reaction of the PMSSQ precursor component, resulting in the phase separation of the porogen component. Such phase separation was found to begin at 393 K for 10 wt% porogen loaded films and at 373 K for 20 wt% porogen loaded films, and then continued for temperatures up to 423 K. These onset aggregation temperatures are relatively lower, compared to those observed in the four-armed poly(ϵ-caprolactone) loaded PMSSQ dielectric films (Lee, Yoon *et al.*, 2005). On the other hand, at higher porogen loadings (≥30 wt%), the PCL6 porogen molecules were found to undergo significant phase separation during the film formation process, resulting in the formation of large porogen aggregates. In summary, this study found that the PCL6 porogen molecules have a tendency to aggregate in the PMSSQ precursor matrix, a tendency that is enhanced as the porogen loading is increased and also as the degree of crosslinking in the PMSSQ precursor component is increased during heating.

Above the onset aggregation temperature, no further phase separation occurred due to the high degree of crosslinking during curing, effectively immobilizing the matrix. The developed porogen aggregates remained confined within the matrix film without any further growth or movement until the temperature reached 564 K (*i.e.* the onset of porogen thermal degradation). At this temperature, the porogens were found to be effectively removed from their individual locations through heating, leaving their individual templates in the film as spherical nanopores. The pore size and size distribution were found to be identical to those of the porogen aggregates prior to thermal degradation. Thus the pore size, size distribution, shape and pore distribution within the PMSSQ film are all governed by the porogen aggregates produced as a result of phase separation, which is induced by curing of the PMSSQ precursor in the range 348–613 K. In addition, the porous dielectric thin film formation process (*i.e.* spin coating, drying and thermal processing) of our study was found to induce no anisotropy in the pore shape and size of the resulting porous films.

This work was supported by the National Research Laboratory (NRL) Program (contract No. 2005-01385) and the Science Research Center (SRC) Program (Center for Integrated Molecular Systems at Postech) of the Korea Science and Engineering Foundation (KOSEF), by the Ministry of Commerce, Industry and Resources (MCIR) and the Ministry of Science and Technology (MOST) (System IC 2010 Project), and by the Korean Ministry of Education (Brain Korea 21 Program). Synchrotron GISAXS measurements were supported by MOST and POSCO Company.

References

Bolze, J., Kim, J., Huang, J.-Y., Rah, S., Youn, H. S., Lee, B., Shin, T. J. & Ree, M. (2002). *Macromol. Res.*, **10**, 2–12.
Bolze, J., Ree, M., Youn, H. S., Chu, S.-H. & Char, K. (2001). *Langmuir*, **17**, 6683–6691.
Czornyj, G., Chen, K. R., Pradasilva, G., Arnold, A., Souleotis, H., Kim, S., Ree, M., Volksen, W., Dawson, D. & DiPietro, R. (1992). *Proc. Electron. Comput. Tech. (IEEE)*, **42**, 682–692.
Kinning, D. J. & Thomas, E. L. (1984). *Macromolecules*, **17**, 1712–1718.
Lee, B., Oh, W., Hwang, Y., Park, Y.-H., Yoon, J., Jin, K. S., Heo, K., Kim, J., Kim, K.-W. & Ree, M. (2005). *Adv. Mater.* **17**, 696–701.

Lee, B., Park, Y.-H., Hwang, Y.-T., Oh, W., Yoon, J. & Ree, M. (2005). *Nature Mater.* **4**, 147–150.
Lee, B., Park, I., Yoon, J., Park, S., Kim, J., Kim, K.-W., Chang, T. & Ree, M. (2005). *Macromolecules*, **38**, 4311–4323.
Lee, B., Shin, T. J., Lee, S. W., Yoon, J., Kim, J. & Ree, M. (2004). *Macromolecules*, **37**, 4174–4184.
Lee, B., Yoon, J., Oh, W., Hwang, Y.-T., Heo, K., Jin, K. S., Kim, J., Kim, K.-W. & Ree, M. (2005). *Macromolecules*, **38**, 3395–3405.
Maex, K., Baklanov, M. R., Shamiryan, D., Iacopi, F., Brongersma, S. H. & Yanovitskaya, Z. S. (2003). *J. Appl. Phys.* **93**, 8793–8841.
Magbitang, T., Lee, V. Y., Miller, R. D., Toney, M. F., Lin, Z., Briber, R. D., Kim, H.-C. & Hedrick, J. L. (2005). *Adv. Mater.* **17**, 1031–1035.
Maier, G. (2001). *Prog. Polym. Sci.* **26**, 3–65.
Morgen, M., Ryan, E. T., Zhao, J.-H., Hu, C., Cho, T. & Ho, P. S. (2000). *Annu. Rev. Mater. Sci.* **30**, 645–680.
Nguyen, C. V., Carter, K. R., Hawker, C. J., Hedrick, J. L., Jaffe, R. L., Miller, R. D., Remenar, J. F., Rhee, H.-W., Rice, P. M., Toney, M. F., Trollsas, M. & Yoon, D. Y. (1999). *Chem Mater.* **11**, 3080–3085.
Oh, W. (2003). PhD thesis, Pohang University of Science and Technology, Republic of Korea.
Oh, W., Hwang, Y.-T., Park, Y. H., Ree, M., Chu, S.-H., Char, K., Lee, J.-K. & Kim, S. Y. (2003). *Polymer*, **44**, 2519–2527.
Pedersen, J. S. (1994). *J. Appl. Cryst.* **27**, 595–608.
Ree, M., Goh, W. H. & Kim, Y. (1995). *Polym. Bull.* **35**, 215–222.
Ree, M. & Ko, I. S. (2005). *Phys. High Tech.* **14**, 2–7.
Ree, M., Yoon, J. & Heo, K. (2006). *J. Mater. Chem.* **16**, 685–697.
Shin, Y. C., Choi, K.-Y., Jin, M. Y., Hong, S.-K., Cho, D., Chang, T. & Ree, M. (2001). *Korea Polymer J.* **9**, 100–106.
Yu, C.-J., Kim, J., Kim, K.-W., Kim, G. H., Lee, H.-S., Ree, M. & Kim, K.-J. (2005). *J. Korean Vac. Soc.* **14**, 138–142.